Research Article

Electrolyte dependent performance of graphene–mixed metal oxide composites for enhanced supercapacitor applications

Remya Simon[1] · Sohini Chakraborty[1] · K. S. Darshini[1] · N. L. Mary[1]

Received: 28 May 2020 / Accepted: 14 October 2020 / Published online: 26 October 2020
© Springer Nature Switzerland AG 2020

Abstract
Graphene–metal frameworks have been extensively studied and developed as electrode materials for next generation energy storage materials. Their high surface area and easily transformable structure enhances its specific capacitance characteristics. In the present study, graphene oxide (GO) was synthesized using Hummers method. Zinc oxide and copper oxide nanoparticles were incorporated in to the GO matrix to form mixed metal oxides. GO, GO–CuO and GO–ZnO were characterized using UV–Visible, FTIR, FT Raman spectroscopy, SEM and XRD to confirm their effective formation. The surface of the glassy carbon electrode was modified by drop casting with the samples on its surface and its electrochemical properties were studied. Cyclic Voltammetry studies were conducted at various scan rates in different electrolytes (KCl, H_2SO_4 and Na_2SO_4) and the characteristic curves were observed to be asymmetric in nature. GO–CuO exhibits the highest specific capacitance of 790 F/g at 5 mV/s in KCl. The specific capacitance of the modified electrodes was also measured using the Chronopotentiometry technique. GO–CuO nanocomposites show a maximum specific capacitance of 800 F/g at 1 A/g. The nanocomposites showed enhanced electrochemical behaviour of the nanocomposites when compared to pure GO. The nanocomposites also showed good cycling stability. The superior performance of the GO–CuO and GO–ZnO nanocomposite electrode renders it as a promising material for supercapacitors applications.

Keywords Nanocomposite · Supercapacitor · Specific capacitance · Graphene oxide

1 Introduction

Development of efficient energy storage devices is a highly pragmatic approach to alleviate the environmental impact of traditional energy resources and rapid increase in global energy consumption. Based on the energy storage mechanism, supercapacitors can be classified into two classes: electric double-layer capacitors (EDLCs) and pseudocapacitors. Usually EDLCs involve porous, carbonaceous materials like graphene, heteroatom (N2,10 B,11 Fe,12 S13) doped graphene and carbon nanotubes while pseudocapacitors solely employ binary, ternary, or even quaternary metal oxides and hydroxides [1].The field of nanotechnology can be viewed as a pioneer in promoting the fabrication of novel supercapacitive materials with a large variety of potential applications [2]. The contact area of the electrode/electrolyte surface per unit mass can be significantly increased by reducing the dimensions to the nanoscale. This will facilitate charge transfer reactions and also introduce more ions to aid the formation of an electrical double layer [3, 4]. Inclusion of properties at the nanoscale will also render new properties such as low weight, transparency, biodegradability and flexibility to supercapacitors which will open new avenues for these

Electronic supplementary material The online version of this article (https://doi.org/10.1007/s42452-020-03708-9) contains supplementary material, which is available to authorized users.

✉ N. L. Mary, maryterrysmc@gmail.com | [1]Department of Chemistry, Stella Maris College (Autonomous) University of Madras, Chennai 600086, Tamil Nadu, India.

devices in the commercial arena. The optimization of the dimension of the material to the nanoscale also leads to tolerance against structural distortion which enables high cycling stability [5]. Transition metal oxides and carbonaceous materials have been extensively used for the fabrication of these devices. The availability of several oxidation states for the redox charge transfer makes transition metal oxides a suitable material for supercapacitor applications [6, 7]. Carbon materials offer the advantage of an inherent double layer, the efficient charging of which is crucial to the performance of the supercapacitor. They also have a high surface area, excellent durability and good mechanical strength. The combination of these two materials to form an asymmetric supercapacitor synergistically enhances the device performance [8–11].

The two-dimensional honeycomb structure of graphene oxide (GO) with exceptional electrical and mechanical properties and large surface area makes it a highly sought after carbonaceous material for the development of supercapacitor [12, 13]. The functionalization of graphene to introduce heteroatoms in its structure leads to the inclusion of pseudo-faradic characteristics which greatly influences the electrical conductivity. Apart from this, functionalization also ensures good wettability and better ionic affinity with the facilitation of good interfacial adhesion between graphene and metal oxide [14]. GO also serves as a conductive porous network for anchoring the uniform distribution of metal oxide nanoparticles. The main drawback of agglomeration of these nanoparticles can be arrested to a great extent by this technique. Zinc oxide with a wide band gap is a promising material for optoelectronic applications. Among metal oxides, zinc oxide and copper oxide is more extensively used in supercapacitor electrodes as they are eco-friendly, possess good electrochemical activity and is more economical when compared to RuO_2 [15–18].

The type, composition and concentration of the electrolyte used are important parameters in determining the electrochemical performance. Aqueous electrolytes are easy to use and do not require controlled environmental conditions [19]. They are also economically viable and non-flammable. Due to their smaller ionic size, they provide low internal resistance, higher conductivity and power density when compared to organic electrolytes. However, the potential window for these electrolytes is limited to around 1 V due to the thermodynamic decomposition of water at 1.3 V [20]. The concentration of the electrolytes also needs to be well optimized to avoid decreased electron transport leading to reduced efficiency. The pH of the aqueous electrolytes can be acidic, basic or neutral. The rate of electron transport decreases with the ionic radius and therefore size of the ions leads to smaller capacitance values. Moreover, effective diffusion of ions in the electrolyte is also an important factor in this respect. The higher the ionic mobility, i.e., greater the ionic character of the electrolyte, higher will be the electron transfer and specific capacitance [21–23].

Here, graphene oxide nanoparticles have been synthesized by Hummer's method. ZnO and CuO have been synthesized by the chemical reduction technique. Nanocomposites of GO/ZnO and GO/CuO have been developed and the samples have been extensively characterized. The electrochemical performance of GO and its nanocomposites have been thoroughly investigated. A comparison is drawn based on the supercapacitive behavior of these electrodes in aqueous solutions of KCl, H_2SO_4 and Na_2SO_4 as electrolytes. The results obtained are evaluated and justified on the basis of the nature of the electrolytes used. An attempt has been made to understand the effect of the composition of these electrolytes on the capacitive behavior of the prepared nanocomposites.

2 Experimental methods

2.1 Materials and experimental methods

2.1.1 Materials

Graphite powder (≥ 99.90%, > 20 µm), sodium nitrate (≥ 99.0%). Potassium permanganate(≥ 85.99%) hydrogen peroxide (≥ 99.92%) sodium hydroxide (≥ 97.0%), potassium hydroxide (≥ 85.99%), zinc nitrate (≥ 99.99%), citric acid (≥ 99.5%) were purchased from Sigma Aldrich. All the materials were used as received without any further purification. Deionized water was used for the experiment.

2.2 Experimental

2.2.1 Preparation of graphene oxide

GO was prepared by using a modified Hummers method which has been reported [24]. Graphite powder (2 g) and $NaNO_3$ (2 g) was added into a beaker with 100 ml of 98 wt% H_2SO_4 at 15 °C for 2 h with continuous stirring and a suspension was obtained. 5 g $KMnO_4$ powder which act as an oxidation agent was gradually added into the suspension with continuous stirring. The process should be maintained in low temperature at below 20 °C for 2 h with continuous stirring. The temperature of the mixture was maintained at room temperature for 48 h with constant stirring after $KMnO_4$ was totally dissolved. 100 ml of deionized water was added into the mixture slowly and a large amount of heat was released. Concentrated H_2SO_4 was diluted and added to the mixture and the temperature was raised to 98 °C.

The solvent was evaporated to dryness for an hour. Scheme 1 gives the schematic representation of the preparation of graphene oxide.

2.3 Preparation of GO/metal oxide

Graphene oxide is dispersed in 100 ml of water by ultrasonication. 0.5 g of M $(NO_3)_2$ (M = Zn, Cu) and 1 g of citric acid are taken in a beaker to which 100 ml of deionized water was added and dissolved. Then the reaction mixture was kept under stirring for 12hrs at 90 °C. The GO/metal oxide is obtained by washing and centrifuging or it can be allowed to evaporate. The product is powdered and stored in the vacuum desiccator. Scheme 2 gives the schematic representation of the preparation of GO/Metal oxide nanoparticles.

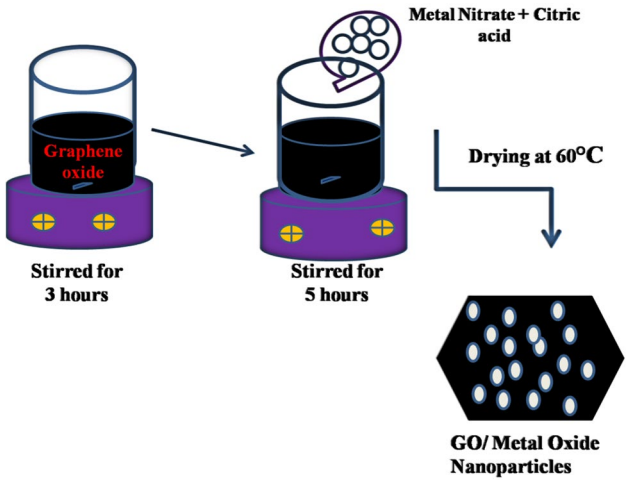

Scheme 2 Schematic representation of the preparation of GO/metal oxide nanoparticles

2.4 Preparation of supercapacitor electrode

GO, GO/ZnO and GO/CuO powered samples were deposited on Glassy Carbon (GC) using the drop casting method. In order to confirm the adhesion of the sample on the GC electrode surface, polytetrafluroethylene (PTFE) was used as the binder. The nanocomposites and PTFE were dissolved in minimum amount of ethanol and 1 mg mL-1 dispersion was prepared by ultrasonication. A micropipette was used to drop cast 1µL of the sample on to the surface of the GC electrode. The electrodes were dried at room temperature and the modified GC electrode was used as the working electrode.

2.5 Material characterization

The absorption spectra of the nanocomposites were recorded by using the Jasco UV–Visible Spectrometer model V-750. Fourier transform infrared spectra (FT-IR) were recorded on a Bruker FTIR Spectrometer (Model Alpha-T) in the range of 400–4000 cm^{-1}. Fourier transform Resonance Raman spectra were conducted using a Bruker RFS Raman spectrophotometer at the range of 50–5000 cm^{-1}. Surface characterization and structural morphology of the samples were analyzed using the FEI Quanta FEG 200- High Resolution Scanning Electron Microscope. X-ray diffraction studies

Scheme 1 Schematic representation of the preparation of graphene oxide powder

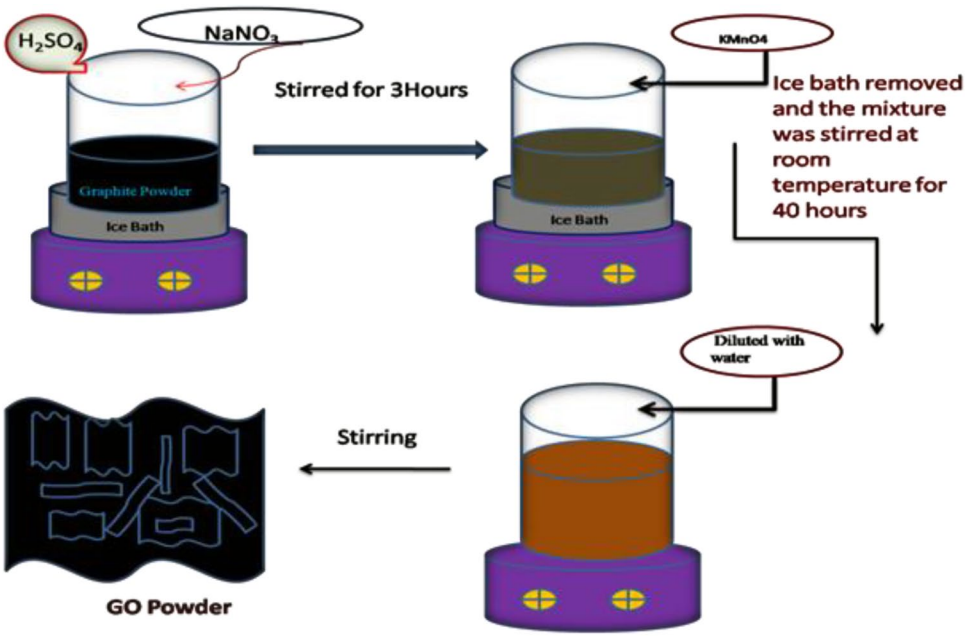

were performed using a Bruker D8 powdered X-ray diffractometer with Cu Kα radiation (λ = 1.5406A).

2.6 Electrochemical characterization

To investigate the capacitive properties of the electrodes, electrochemical impedance spectrometry (EIS), cyclic voltammetry (CV) and chronopotentiometry (CP) experiments were performed using a CHI 608 E Electrochemical workstation in a three electrode mode, including a platinum wire as the counter electrode, standard calomel electrode as a reference electrode and glassy carbon as working electrode. The experiments were run at room temperature with different electrolytes such as 0.5 M KCl, H_2SO_4 and Na_2SO_4.

Cyclic voltammetry studies were performed in 0.5 M KCl, H_2SO_4 and Na_2SO_4 solution with scan rates ranging from 5 to100 mVs^{-1}. The specific capacitance was calculated from the CV using the formula [25]:

$$Cv = \frac{\int_{V1}^{V2} idV}{V \times m \times (V2 - V1)} \quad (1)$$

where i = instant current (A), m = mass of electrode (g), V = potential scan rate (V/s), V1 = high potential of CV (V), V2 = low potential of CV (V) and Cv is the specific capacitance (F/g).

Charge discharge measurements were carried out in the potential window of − 0.4–0.8 V at different current densities (1, 2, 3, 4, 5 and 6A/g). The specific capacitance of the electrode materials was evaluated from the discharge curves using the Eq. (2):

$$Csp = I\,\Delta t / m\,\Delta V \quad (2)$$

where m is the loading mass (g), C_{sp} is the specific capacitance (F/g), I is the discharge current (A), ΔVis the voltage change (V) and Δt is the discharge time (s) of the electrode materials during the discharge process. The energy density (E, Wh/kg) and power density (P,kWh/kg) of the supercapacitor were estimated using Eqs. (3,4):

$$E = Csp\Delta V2/2 * 3.6 \quad (3)$$

$$P = (E * 3600)/\Delta t \quad (4)$$

3 Result and discussion

3.1 Spectral studies

3.1.1 Fourier transform Raman spectroscopy

Raman spectra of GO, GO–CuO and GO–ZnO composites are illustrated in Fig. 1. The Raman spectrum of graphene is usually characterized by two main modes of vibrations, G and D. G band arises due to the breathing mode of k-point phonons of A1g symmetry. It can be observed that all the three materials show a peak at 1332 cm^{-1} (GO), 1316 cm^{-1} (GO–CuO) and 1270 cm^{-1} (GO–ZnO) which can be attributed to the D band associated with the structural defects that are related to the partially disordered structure of the D band associated with the structural defects that are related to the partially disordered structure of the graphitic domains or the attachments of the functional groups on the carbon basal plane [25]. The peaks at 1576 cm^{-1} (GO), 1593 cm^{-1} (GO–ZnO) and 1578 cm^{-1} (GO–CuO) correspond to the G band, which arises from the first-order scattering of the E_{2g} phonon of the sp^2 carbon atoms. In GO–ZnO, additional peaks at 434, 578 and 1095 cm^{-1}, are due to the ZnO nanostructures anchored onto the GO surface. The characteristic peak at 434 cm^{-1} belongs to E_2 high mode of vibrations in ZnO, indicating the wurtzite crystal phase of attached ZnO nanostructures. The peak at 578 cm^{-1} can be assigned to the E1 low mode of vibrations corresponding to the oxygen deficiency defect in ZnO. The peak at 1095 cm^{-1} can be attributed to the multiple phonon scattering processes in ZnO. There are Raman peaks at 290, 322 and 614 cm^{-1} in GO–CuO which can be assigned to one A_g and two B_g modes, respectively [26].

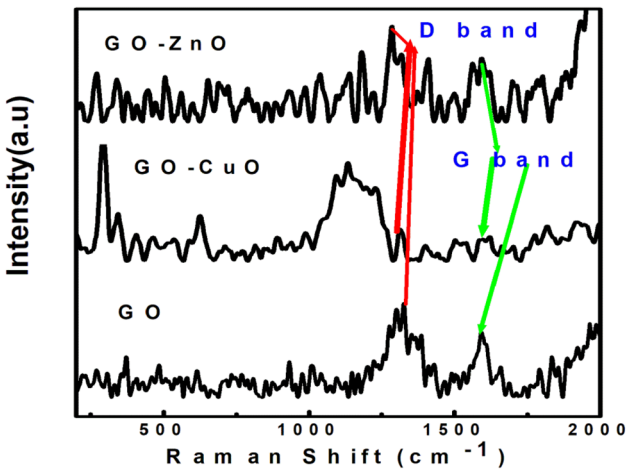

Fig. 1 FT-Raman spectra of different nanocomposites

The intensity ratio of D peak to G peak (I_D/I_G) is 1.30 for GO–ZnO, 1.27 for GO–CuO and 1.34 for pure GO. GO–CuO and GO–ZnO are not purely sp^2 in nature. It can be observed that the ratio of I_D/I_G is very low for GO–CuO and GO–ZnO when compared to GO. An increase of I_D/I_G is due to a decrease in the overall sp^2 conjugation. CuO and ZnO interacts with GO differently. The SEM images also show that ZnO is more effectively distributed and it interacts more with the layers of GO than CuO. Thus, the sp^2 character is compromised more in case of GO–ZnO than GO–CuO leading to an increase in the I_D/I_G ratio [27].

3.1.2 X- Ray diffraction (XRD) analysis

Figure 2 shows the XRD patterns of GO, GO–ZnO and GO–CuO nanocomposites. Characteristic carbon peak corresponding to the (001) plane for the GO sheets appear at 10°. After addition of ZnO and CuO, (001) eventually disappears and new peaks at (100) and (002) was observed at two theta values of 25.42° and 26.40°respectively. The diffraction peak of GO–CuO was observed at two theta values of 32.70°, 36.10°, 39.50°, 40.30° and 42.40° correspond to the (110), (111),(200),(112),(202) and (113) planes respectively. The pattern shows the formation of monoclinic CuO phase (JCPDS Card No. 80–1916) [28]. In the case of GO–ZnO, the diffraction peaks at 32.29°, 35.29°, 37.49°, 41.04°, 48.08° and 53.02° correspond to the (100),(102),(002),(011),(012) and (013) planes respectively and it was observed that ZnO has a hexagonal structure (JCPDS 65–433,411) [29].

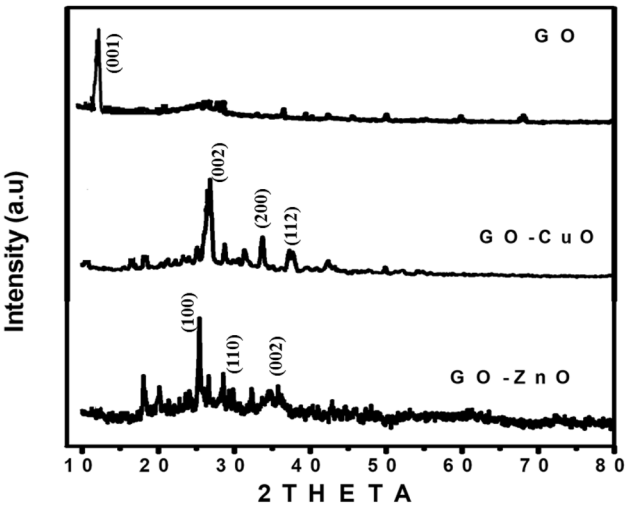

Fig. 2 XRD patterns of different nanocomposites

From Fig. 2, the average crystallite size of the GO, GO–ZnO and GO–CuO was calculated from the Scherrer equation:

$$D = k\lambda / \beta \cos\theta$$

where D = average crystallite size, λ = Wavelength of incident X-ray beam (1.5406Å), β = Bragg's diffraction angle.

The crystallite size for GO, GO–ZnO and GO–CuO are 40.028, 35.45 and 66.68 nm and its lattice strains were 0.00326, 0.0156 and 0.0023 respectively.

3.1.3 Scanning electron microscopy (SEM)

The scanning electron microscopic studies have been performed to study the morphology and compatibility between the various components. Figure 3 shows the SEM image of the nanoparticle and its nanocomposites. SEM image of GO show the flat surface with ordered layer structure [30]. Graphene oxide reveals randomly aggregated, thin, crumpled layers structure. It exhibits that the oeiented layer structure of graphite has been unbalanced due to its oxidation. The graphite sheets have exfoliated into mono or multi- layer graphene oxide sheet [31]. GO–ZnO and GO–CuO shows effectual incorporation of the ZnO and CuO nanoparticles with no significant cluster formation in the matrix. This can be attributed to sonication over long periods of time thereby ensuring dispersion of these nanoparticles into the graphene oxide sheet.

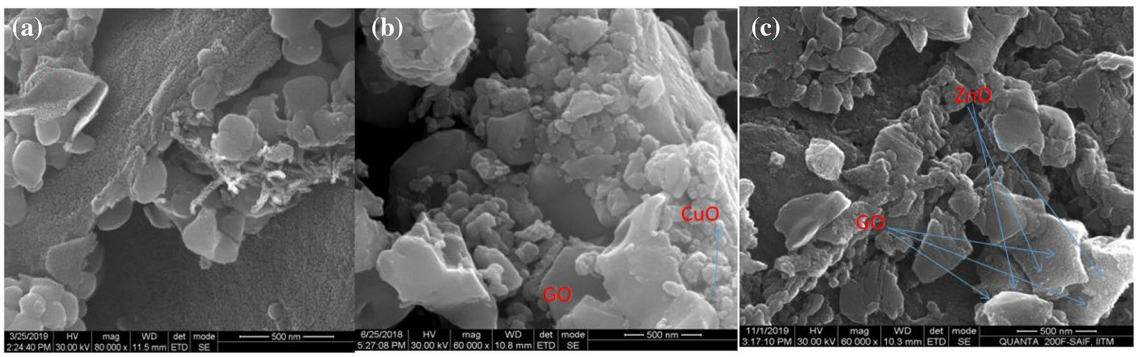

Fig. 3 SEM image of **a** GO, **b** GO–CuO and **c** GO–ZnO

Figure 4 shows energy dispersive X-ray spectroscopy (EDAX) analysis of the nanocomposites incorporated with CuO and ZnO nanoparticles. Elemental mapping confirmed that carbon, oxygen, zinc and copper are the constituent elements of the nanocomposite. This distribution and effective incorporation of Zinc and Copper oxide

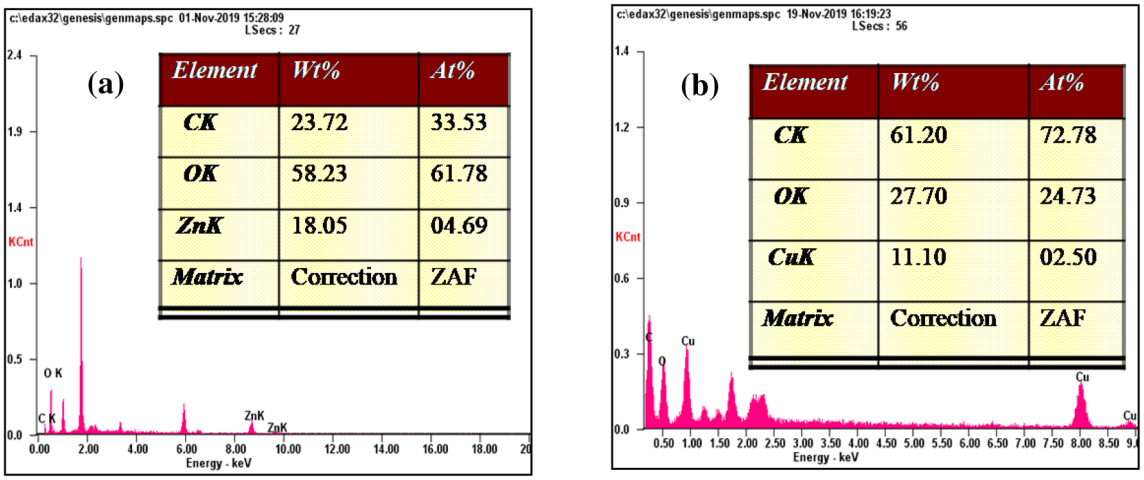

Fig. 4 EDAX of **a** GO–ZnO and **b** GO–CuO

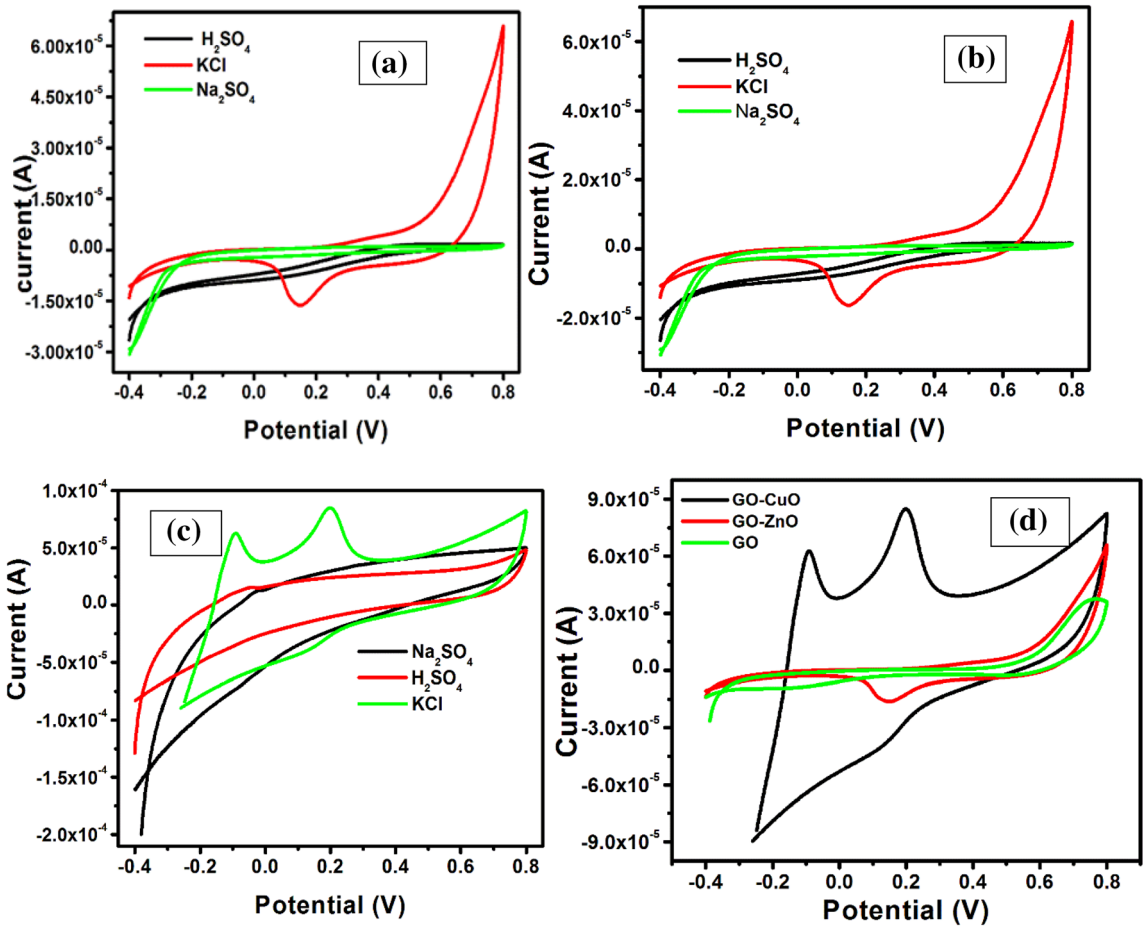

Fig. 5 Cyclic voltammograms of **a** GO–CuO, **b** GO–ZnO, **c** GO at 5 mVs^{-1} in different electrolytes and **d** Comparative study of various samples in 0.5 M KCl

nanoparticles into the graphene oxide sheet can be further reaffirmed by its weight percentages of 15.27% and 11.10% respectively from the EDAX analysis.

3.2 Electrochemical properties of graphene metal oxide nanocomposites

3.2.1 Cyclic voltammogram (CV)

Figure 5 shows the CV of the samples in 0.5 M KCl, H_2SO_4 and Na_2SO_4 recorded at 5mVs^{-1} scan rate. The shape of the curves clearly reveals the asymmetric supercapacitive characteristics of the nanocomposites. The linear increase of current in different electrolytes exhibits the enhanced capacitive behavior of the GO–CuO and GO–ZnO electrodes. The presence of redox peaks in the voltammograms can be attributed to the psuedocapacitive behaviour of the metal oxides [4]. From the CV, it can be confirmed that the ionic electrolyte (KCl) displayed the highest current response than any other electrolyte. The specific capacitance of GO, GO–ZnO and GO–CuO electrodes can be calculated from the CV curves shown in Fig. 6. On comparing the C_{sp} values listed in Table 1, it was revealed that the supercapacitive performance of GO–CuO is higher than that of the neat GO electrode and hence the enhancement of charge storage ability due to CuO nanoparticles incorporation on the graphene oxide sheet is confirmed [31]. The highest capacitance of GO–CuO was 790 F/g at a scan rate of 5 mVs^{-1} in KCl and GO, GO–ZnO has a capacitance value of 332 and 445 F/g respectively at the same scan rate using the same electrolyte. KCl is a strongly ionic electrolyte and therefore the dissociation of ions takes place at a faster rate for KCl. This ensures a rapid surge in ionic mobility of the electrolyte thereby resulting in a more efficient ionic diffusion leading to higher capacitance values. The peak to peak separation in different electrolytes indicates a dependence on the voltage scan rate and the electrochemical

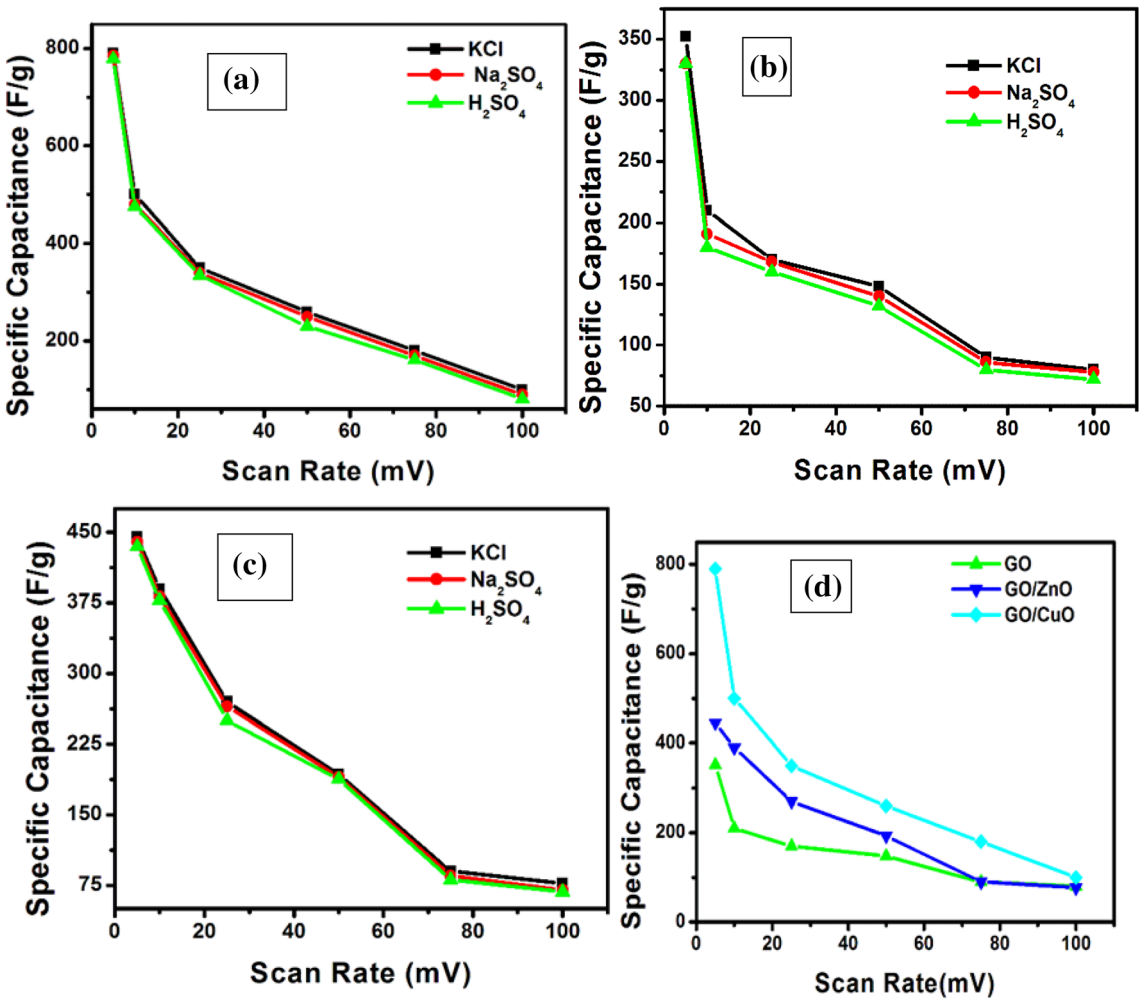

Fig. 6 Specific capacitances of **a** GO, **b** GO–ZnO, **c** GO–CuO in different electrolytes and **d** Comparative study of various samples at 0.5 M KCl

Table 1 Specific capacitance values of various samples in different electrolytes

Code	ScanRate(mVs^{1})	Specificcapacitance in KCl (F/g)	Specificcapacitance in Na_2SO_4 (F/g)	Specific capacitance in H_2SO_4(F/g)
GO	5	352	330	330
	10	210	191	180
	25	170	168	160
	50	148	140	132
	75	90	86	80
	100	80	78	72
GO–ZnO	5	445	440	435
	10	390	382	378
	25	270	265	250
	50	193	190	188
	75	90	85	81
	100	81	70	68
GO–CuO	5	790	785	779
	10	500	480	475
	25	350	340	335
	50	260	250	230
	75	180	170	161
	100	100	90	81

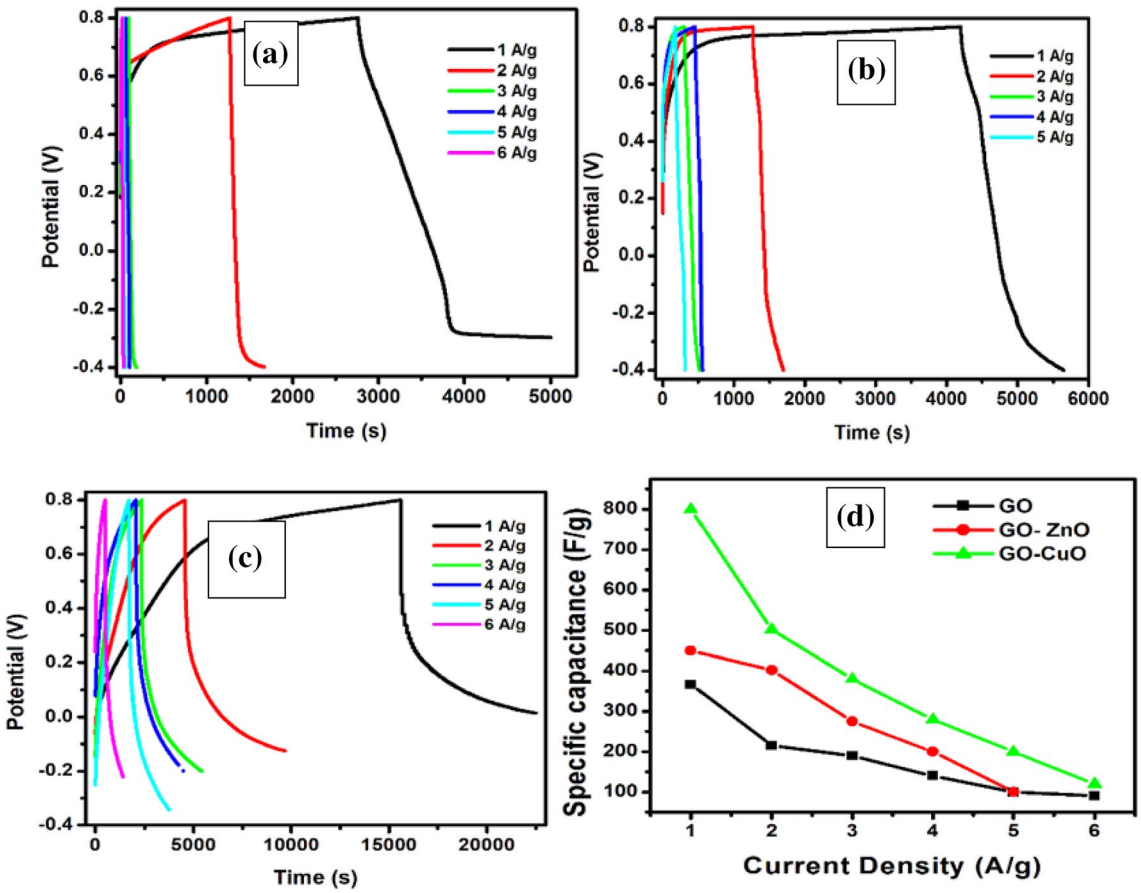

Fig. 7 Chronopotentiometry of **a** GO, **b** GO–ZnO, **c** GO–CuO and **d** Specific capacitance of various samples

Table 2 Specific capacitance values of various samples from the charge discharge curve

CODE	Current Density(A/g)	Specific capacitance(F/g)
GO	1	367
	2	215
	3	190
	4	140
	5	100
	6	100
GO–ZnO	1	450
	2	402
	3	275
	4	200
	5	150
GO–CuO	1	800
	2	502
	3	380
	4	280
	5	200
	6	120

process can be classified as quasi-reversible within the scan rate employed [32].

3.2.2 Chronopotentiometry (CP)

The electrochemical properties of GO, GO–ZnO and GO–CuO were characterized in three electrode configurations with 0.5 M KCl ionic aqueous solution as electrolyte. Figure 7 represents a typical charge discharge curve of different samples atvarious current densities which shows a triangular fashion and corresponds to the electrochemical behavior of asymmetric supercapacitors [33]. The CP was investigated from -0.4 to 0.8 V at different densities of 1, 2, 3, 4, 5 and 6 A/g. On comparing the C_{sp} values listed in Table 2, it was revealed that the supercapacitive performance of GO–CuO is greater than that of the pure GO electrode, and hence the enhancement of charge storage ability due to incorporation of CuO nanoparticlesis confirmed. The capacitance of GO–CuO was 800 F/g at a current density of 1.0 A/g and GO–ZnO has a capacitance value of 450 F/g at the same current density. The obtained

Table 3 Typical specific capacitance of various reported GO–MO systems (M = Zn, Cu)

Electrode material	Electrolyte	Specific Capacitance(Fg^{-1})	Voltage Range(V)	Measured condition	References
rGO@CuxO	2 M KOH	267.2	– 1.0–0 V	2 A/g	[34]
GO–CuO nanocomposites	1 M Na_2SO_4	245	0–0.8	0.1 A/g	[35]
3DCuO/GOA	1 M Na_2SO_4	211	0.6–0.6	1 A/g	[36]
CuO–graphene	6 M KOH	305	0–0.4	2 A/g	[37]
PPy/GO/ ZnO	6 M KOH	123	0.0–0.9	1 A/g	[38]
GNS/ZnO composite	1 M KOH	62	– 0.6–0.2	10 mA/g	[39]
ZnO/rGO composite	1 M Na_2SO_4	180	0–1.0	4A/g	[40]
GO–ZnO	0.5 M KCL	450	– 0.4–0.8	1A/g	Present work
GO–CuO	0.5 M KCL	800	– 0.4–0.8	1A/g	Present work

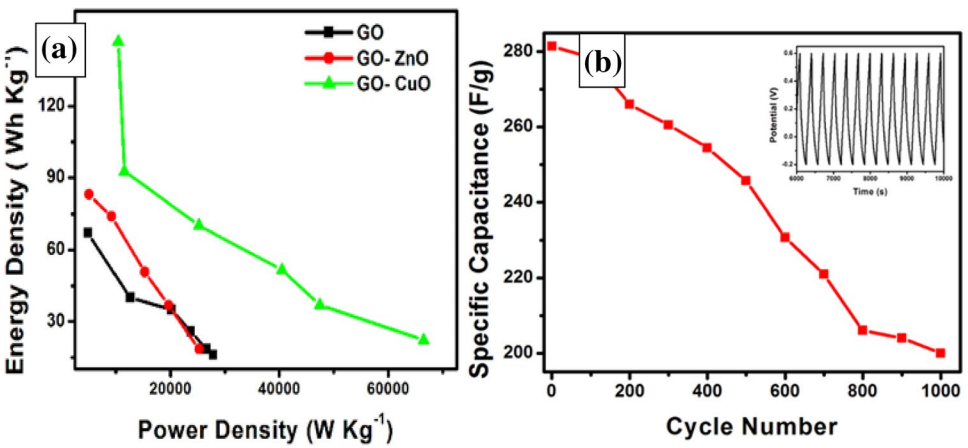

Fig. 8 **a** Ragone plots of the samples and **b** Specific capacitance verses Cycle Number of GO–CuO

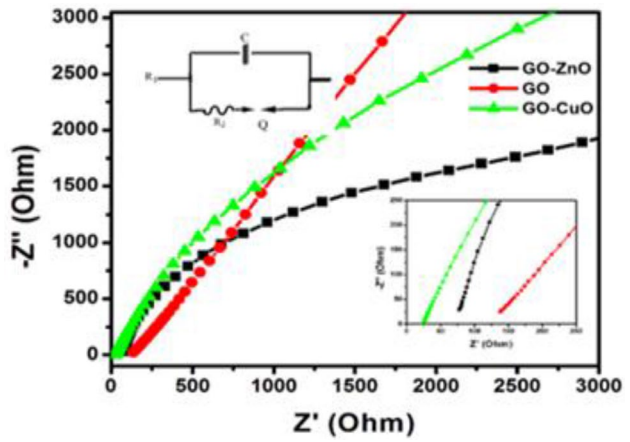

Fig. 9 Impedance spectra of the nanocomposites fitted using the equivalent circuit model

Table 4 Fitting parameters as obtained for the nanocomposites

Sample code	R_1 (Ωcm^2)	R_2 (Ωcm^2)	Q (Fcm^2)	C (Fcm^2)
GO	82	853	0.0000589	0.00000099
GO–ZnO	135.5	84.91	0.0000145	0.0000007
GO–CuO	140	50	0.0000025	0.0000004

Specificcapacitance in the present work have been compared with those from earlier works (Table 3).

Moreover, the GO–CuO displays a high energy density of 147 kg^{-1} at a power density of 10,425 Wkg^{-1} and 22.15 Wh kg^{-1} at a high power density of 66,450 Wkg^{-1} (Fig. 8a). The cycling stability of GO–CuO have been carried out at 4 A/g for 1000 segments and it shows 71% capacitance retention after 1000 segments as depicted in Fig. 1b.

3.2.3 Electrochemical Impedance spectroscopy (EIS)

Figure 9 exhibits the impedance spectra of the nanocomposites. To further re-establish the enhanced supercapacitive performance of the nanocomposites, a comparative study of EIS between the characteristics of pristine GO electrode and the GO–ZnO and GO–CuO composite electrode has been proposed. Among the graphene / metal oxide composites, the vertical curve of GO–CuO has the largest slope with respect to the Z'axis, i.e., it is the closest to the imaginary impedance axis (Z'') which implies that GO–CuO exhibits the highest conductivity or lowest internal resistance [41]. An equivalent circuit was employed to further analyze the obtained Nyquist plots using the Zsimp Win software (version 3.21). In this model, R_1 is the solution resistance of supercapacitors, R_2 is the charge transfer resistance, Q represents the constant phase potential and C is the capacitance. The fitting parameters are listed in Table 4. From the table it can be observed that, GO–CuO has a lowest charge transfer resistance followed by GO–ZnO and GO which confirms the highest conductivity of GO–CuO.

4 Conclusion

Graphene oxide incorporated with ZnO and CuO was successfully prepared and GO–CuO and GO–ZnO nanocomposites have been established as a promising electrode material for supercapacitors. The structural, morphological and compositional analysis using XRD, HR-SEM, EDAX, FTIR and FT Raman spectroscopy have confirmed the formation of the Graphene—metal oxide nanocomposites. The highest value of 800 F/g specific capacitance was observed for GO–CuO nanocomposites at a current density of 1 A/g. After 1000 charge discharge cycles, GO–CuO shows good cycling stability. From the enhanced electrochemical behavior of the nanocomposites, it can be inferred that this material has a huge potential to be used as a supercapacitor electrode material. Therefore, it can be established that existing electrode materials can be tailored to extend their application window for use as efficient electrochemical energy storage agents. This study be further extended to other transition metal oxides based electrodes for supercapacitor applications and the results can be compared.

Acknowledgements We would like to thank the DST-FIST programme-2015 LEVEL 0 for providing us with the instrumentation facilities to carry out this research work. We are grateful to the Centre for Research in Science and Technology (CRIST), Stella Maris College, Chennai for helping us with the characterisation of the samples.

Compliance with ethical standard

Conflicts of interest The authors declare that they have no conflicts of interest.

References

1. Zhao X, Hayner CM, Kung MC, Kung HH (2011) Flexible holey graphene paper electrodes with enhanced rate capability for energy storage applications. ACS Nano 5:8739–8749
2. Lv Z, Li W, Yang L, Loh XJ, Chen X (2019) Custom-made electrochemical energy storage devices. ACS Energy Lett 4:606–614
3. Chen C, Hu L (2018) Nanocellulose toward advanced energy storage devices: structure and electrochemistry. Acc Chem Res 51:3154–3165
4. Halder L et al (2019) Fabrication of an advanced asymmetric supercapacitor based on three-dimensional copper–nickel–cerium–cobalt quaternary oxide and GNP for energy storage application. ACS Appl Electron Mater 1:189–197
5. Şen B et al (2017) Bimetallic PdRu/graphene oxide based catalysts for one-pot three-component synthesis of

2-amino-4H-chromene derivatives. Nano-Struct Nano-Objects 12:33–40
6. Anjum SR, Narwade VN, Bogle KA, Khairnar RS (2018) Graphite doped Hydroxyapatite nanoceramic: selective alcohol sensor. Nano-Struct Nano-Objects 14:98–105
7. Ghosh S et al (2017) Supercapacitive vertical graphene nanosheets in aqueous electrolytes. Nano-Struct Nano-Objects 10:42–50
8. Hitkari G, Singh S, Pandey G (2017) Structural, optical and photocatalytic study of ZnO and ZnO–ZnS synthesized by chemical method. Nano-Struct Nano-Objects 12:1–9
9. Sarkar C, Dolui SK (2015) Synthesis of copper oxide/reduced graphene oxide nanocomposite and its enhanced catalytic activity towards reduction of 4-nitrophenol. RSC Adv 5:60763–60769
10. Yaragalla S, Rajendran R, AlMaadeed MA, Kalarikkal N, Thomas S (2019) Chemical modification of graphene with grape seed extract: Its structural, optical and antimicrobial properties. Mater Sci Eng C 102:305–314
11. Palussiere S et al (2019) The role of alkylamine in the stabilization of CuO nanoparticles as a determinant of the Al/CuO redox reaction. Phys Chem Chem Phys 21:16180–16189
12. You B, Li N, Zhu H, Zhu X, Yang J (2013) Graphene oxide-dispersed pristine CNTs support for MnO2 nanorods as high performance supercapacitor electrodes. Chemsuschem 6:474–480
13. Maiti UN, Lim J, Lee KE, Lee WJ, Kim SO (2014) Three-dimensional shape engineered, interfacial gelation of reduced graphene oxide for high rate, large capacity supercapacitors. Adv Mater 26:615–619
14. Nongthombam S et al (2020) Reduced graphene oxide/gallium nitride nanocomposites for supercapacitor applications. J Phys Chem Sol 141:345
15. Wu F, Harper BJ, Crandon LE, Harper SL (2020) Assessment of Cu and CuO nanoparticle ecological responses using laboratory small-scale microcosms. Environ Sci Nano 7:105–115
16. Banerjee P, Jain PK (2018) Mechanism of sulfidation of small zinc oxide nanoparticles. RSC Adv 8:34476–34482
17. Kumar N, Pathak TK, Purohit LP, Swart HC, Goswami YC (2018) Self-assembled Cu doped CdS nanostructures on flexible cellulose acetate substrates using low cost sol–gel route. Nano-Struct Nano-Objects 16:1–8
18. Senthilkumar V et al (2015) Comparative supercapacitance performance of CuO nanostructures for energy storage device applications. RSC Adv 5:20545–20553
19. Mahjani MG, Ehsani A, Jafarian M (2010) Electrochemical study on the semiconductor properties and fractal dimension of poly ortho aminophenol modified graphite electrode in contact with different aqueous electrolytes. Synth Met 160:1252–1258
20. Weissmann M, Crosnier O, Brousse T, Bélanger D (2012) Electrochemical study of anthraquinone groups, grafted by the diazonium chemistry, in different aqueous media-relevance for the development of aqueous hybrid electrochemical capacitor. Electrochim Acta 82:250–256
21. Van Aken KL, Beidaghi M, Gogotsi Y (2015) Formulation of ionic-liquid electrolyte to expand the voltage window of supercapacitors. Angew Chemie - Int Ed 54:4806–4809
22. Jiang M et al (2016) Poly(vinyl Alcohol) borate gel polymer electrolytes prepared by electrodeposition and their application in electrochemical supercapacitors. ACS Appl Mater Interfaces 8:3473–3481
23. Maheswari N, Muralidharan G (2015) Supercapacitor behavior of cerium oxide nanoparticles in neutral aqueous electrolytes. Energy Fuels 29:8246–8253
24. Singh RK, Kumar R, Singh DP (2016) Graphene oxide: strategies for synthesis, reduction and frontier applications. RSC Adv 6:64993–65011
25. Zheng F, Xu WL, Jin HD, Hao XT, Ghiggino KP (2015) Charge transfer from poly(3hexylthiophene) to graphene oxide and reduced graphene oxide. RSC Adv 5:89515–89520
26. Jilani SM, Banerji P (2014) Graphene Oxide—Zinc oxide nanocomposite as channel layer for field effect transistors: effect of ZnO loading on field effect transport. ACS Appl Mater Interfaces 10:1–8
27. Zhu J (2010) Decorating graphene oxide with CuO nanoparticles in a water-isopropanol system. Nanoscale 2:988–994
28. Long C, Wei T, Yan J, Jiang L, Fan Z (2013) Supercapacitors based on graphene-supported iron nanosheets as negative electrode materials. ACS Nano 7:11325–11332
29. Liu X et al (2012) UV-assisted photocatalytic synthesis of ZnO-reduced graphene oxide composites with enhanced photocatalytic activity in reduction of Cr(VI). Chem Eng J 183:238–243
30. Saleem H, Haneef M, Abbasi HY (2018) Synthesis route of reduced graphene oxide via thermal reduction of chemically exfoliated graphene oxide. Mater Chem Phys 204:1–7
31. Chakraborty S, Mary NL (2020) A carbon nanotube reinforced functionalized styrene-maleic anhydride copolymer as an advanced electrode material for efficient energy storage applications. New J Chem 44:4406–4416
32. Chen R, Yu S, Sun R, Yang W, Zhao Y (2012) KCl-assisted, chemically reduced graphene oxide for high-performance supercapacitor electrodes. J Sol State Electrochem 16:3635–3641
33. Chakraborty S, RMary MANL (2020) Biocompatible supercapacitor electrodes using green synthesised ZnO/Polymer nanocomposites for efficient energy storage applications. J Energy Storage 28:101275
34. Jafari EA, Moradi M, Hajati S, Kiani MA, Espinos JP (2018) Electrophoretic deposition of mixed copper oxide/GO as cathode and N-doped GO as anode for electrochemical energy storage. Electrochim Acta 268:392–402
35. Pendashteh A, Mousavi MF, Rahmanifar MS (2013) Fabrication of anchored copper oxide nanoparticles on graphene oxide nanosheets via an electrostatic coprecipitation and its application as supercapacitor. Electrochim Acta 88:347–357
36. Song Z et al (2019) One-step self-assembly fabrication of three-dimensional copper oxide/graphene oxide aerogel composite material for supercapacitors. Solid State Commun 287:27–30
37. Zhao B et al (2013) Hierarchical self-assembly of microscale leaf-like CuO on graphene sheets for high-performance electrochemical capacitors. J Mater Chem A 1:367–373
38. Sarkar J, Bhattacharyya S (2012) Application of graphene and graphene-based materials in clean energy-related devices Minghui. Arch Thermodyn 33:23–40
39. Wang J et al (2011) Green synthesis of graphene nanosheets/ZnO composites and electrochemical properties. J Solid State Chem 184:1421–1427
40. Chen YL et al (2011) Zinc oxide/reduced graphene oxide composites and electrochemical capacitance enhanced by homogeneous incorporation of reduced graphene oxide sheets in zinc oxide matrix. J Phys Chem C 115:2563–2571
41. Akhina H, Mohammed Arif P, Gopinathan Nair MR, Nandakumar K, Thomas S (2019) Development of plasticized poly (vinyl chloride)/reduced graphene oxide nanocomposites for energy storage applications. Polym. Test. 73:250–257

Publisher's Note Springer Nature remains neutral with regard to jurisdictional claims in published maps and institutional affiliations.